Journal of Applied Physics

# Comparative band alignment of plasma-enhanced atomic layer deposited high-k dielectrics on gallium nitride

Cite as: J. Appl. Phys. **112**, 053710 (2012); https://doi.org/10.1063/1.4749268
Submitted: 15 May 2012 • Accepted: 31 July 2012 • Published Online: 07 September 2012

**Jialing Yang, Brianna S. Eller, Chiyu Zhu, et al.**

# Comparative band alignment of plasma-enhanced atomic layer deposited high-k dielectrics on gallium nitride

Jialing Yang, Brianna S. Eller, Chiyu Zhu, Chris England, and Robert J. Nemanich
*Department of Physics, Arizona State University, Tempe, Arizona 85287-1504, USA*

(Received 15 May 2012; accepted 31 July 2012; published online 7 September 2012)

$Al_2O_3$ films, $HfO_2$ films, and $HfO_2/Al_2O_3$ stacked structures were deposited on n-type, Ga-face, GaN wafers using plasma-enhanced atomic layer deposition (PEALD). The wafers were first treated with a wet-chemical clean to remove organics and an *in-situ* combined $H_2/N_2$ plasma at 650 °C to remove residual carbon contamination, resulting in a clean, oxygen-terminated surface. This cleaning process produced slightly upward band bending of 0.1 eV. Additional 650 °C annealing after plasma cleaning increased the upward band bending by 0.2 eV. After the initial clean, high-k oxide films were deposited using oxygen PEALD at 140 °C. The valence band and conduction band offsets (VBOs and CBOs) of the $Al_2O_3$/GaN and $HfO_2$/GaN structures were deduced from *in-situ* x-ray and ultraviolet photoemission spectroscopy (XPS and UPS). The valence band offsets were determined to be 1.8 and 1.4 eV, while the deduced conduction band offsets were 1.3 and 1.0 eV, respectively. These values are compared with the theoretical calculations based on the electron affinity model and charge neutrality level model. Moreover, subsequent annealing had little effect on these offsets; however, the GaN band bending did change depending on the annealing and processing. An $Al_2O_3$ layer was investigated as an interfacial passivation layer (IPL), which, as results suggest, may lead to improved stability, performance, and reliability of $HfO_2$/IPL/GaN structures. The VBOs were ~0.1 and 1.3 eV, while the deduced CBOs were 0.6 and 1.1 eV for $HfO_2$ with respect to $Al_2O_3$ and GaN, respectively. © *2012 American Institute of Physics*. [http://dx.doi.org/10.1063/1.4749268]

## I. INTRODUCTION

GaN-based transistors have shown great potential in a broad spectrum of electronics applications, including high frequency, high power, and high temperature electronics, due to their excellent properties such as a high saturation velocity and high breakdown field. However, the relatively high gate leakage is one of the major factors that limit the performance and reliability of GaN based transistors.[1] This limitation is significantly mitigated with the use of metal/high-k oxide/III-N structures, which lowers the leakage current and improves the thermal stability. As a result, high-k oxides have gained considerable attention from researchers who have investigated the use of various dielectrics as gate insulators including $Al_2O_3$,[1–5] $HfO_2$,[6–8] $ZrO_2$,[9] $Sc_2O_3$,[10–13] MgO,[11,14–16] $Gd_2O_3$,[17] and $Ga_2O_3(Gd_2O_3)$.[18–20] However, these dielectrics in the current processes are not ready for low-cost or high-yield manufacturing, which is largely a result of the deposition method.[1] Atomic layer deposition (ALD) is a robust and highly manufacturable method, which relies on self-limiting adsorption to control the layer-by-layer deposition of the high-k material. This method is based on sequential gas phase exposure and surface chemical processes. The organometallic precursor and reactive gas—separated by a purging gas—are delivered into the chamber, where they react at the sample surface in a cyclic manner to form a thin film. This method not only increases uniformity and nanometer control but also decreases defect densities when compared to other deposition methods such as sputtering and electron-beam deposition. By using activated oxygen species generated by a plasma, plasma-enhanced ALD (PEALD) can not only significantly reduce the deposition temperature but also reduce the impurities and increase the growth rate and film density.[21]

To advance the current understanding, we have used plasma-enhanced ALD to investigate two promising high-k dielectrics, aluminum oxide ($Al_2O_3$), and hafnium oxide ($HfO_2$). In comparison, $Al_2O_3$ has a larger band gap (~6.5 eV),[22,23] stronger adhesion to many surfaces, and better chemical and thermal stabilities than $HfO_2$. The large band gap provides a sufficient barrier for carriers in the GaN valence and conduction bands; however, $Al_2O_3$ also has a relatively low dielectric constant (~9), which limits further scaling of the equivalent oxide thickness (EOT). $HfO_2$, on the other hand, has a high dielectric constant (~20), which can decrease the EOT in comparison with $Al_2O_3$, but $HfO_2$ is not as stable as $Al_2O_3$.[24,25] Furthermore, the relatively narrow band gap associated with hafnium oxide (~5.8 eV) would not limit the leakage current as effectively and thus affect device performance. Considering the complementary characteristics of $Al_2O_3$ and $HfO_2$, devices could achieve lower leakage current and higher thermal stability by using $Al_2O_3$ as an interfacial passivation layer (IPL) between the semiconductor substrate and $HfO_2$.[24]

Previous research has focused primarily on the preparation and cleaning of GaN surfaces using HCl, TCE, and annealing as well as various hydrogen and nitrogen treatments.[26–29] There has also been some investigation into band alignment of the dielectric/GaN interface with $HfO_2$ grown via molecular beam deposition (MBD).[8] The band alignment

 

characteristics play a critical role in determining the confinement properties of carriers in the semiconductor and ultimately the performance of electronic and optoelectronic devices. This study focuses on the band-alignment of the $Al_2O_3$/GaN, $HfO_2$/GaN, and $Al_2O_3$/$HfO_2$/GaN stacked structures grown via PEALD. Results for the surface band bending of the oxygen-terminated, Ga-face GaN are consistent with other experimental studies and reveal that an additional annealing during the cleaning process increases the upward band bending. These measurements are well below the values expected based on the polarization bound charge and doping level. Apparently, structural defects, surface contamination, and surface states contribute to Fermi level pinning or additional charge compensation, which screen the polarization charge. The results for the band alignment of the $Al_2O_3$ and $HfO_2$ thin films are discussed in terms of the electron affinity and charge neutrality level models. The results of the stacked structure of $HfO_2$/$Al_2O_3$/GaN are also discussed. In addition to the band alignment of these interfaces, the effects of plasma treatment are also noted.

## II. EXPERIMENT

### A. Cleaning

The $5 \pm 1\,\mu$m thick, n-type, Ga-face, epitaxial, GaN wafers—obtained from and diced by READE Advance Materials—were grown via HVPE on sapphire substrates. The GaN doping density $N_D$ is $\sim 1 \times 10^{17}\,cm^{-3}$, which determines the GaN Fermi level at 0.1 eV below the conduction band minimum. Prior to ALD deposition, the wafer sections were treated with an *ex-situ* wet-chemical clean. This process includes sonicating the wafer in separate acetone, methanol, and HCl acid baths for 10 min each; the acetone and methanol remove organics, while the HCl reduces carbon and oxygen contamination on the surface.[27] An *in-situ* remote plasma clean was employed to remove remaining carbon contamination and reduce the surface defect density. The samples were exposed to an *in-situ* combined $H_2$ and $N_2$ (1:4) plasma treatment at 650 °C for 15 min, where the pressure and combined gas flow rate were maintained at 60 mTorr and 90 standard cubic centimeter per minute (sccm), respectively.

### B. Plasma-enhanced atomic layer deposition

After cleaning, the sample was transferred in ultra high vacuum (UHV) to the PEALD system. A schematic illustration of the system is shown in Fig. 1. The background pressure in the chamber was $\sim 6.0 \times 10^{-9}$ Torr. During deposition, the ALD software controlled the pulse time of the gases. During a 0.1 s precursor pulse, the precursor was delivered into the chamber with an argon carrier gas. This pulse was followed by 10 s of $N_2$ gas, used to purge excess precursor from the chamber. Then, $O_2$ gas was introduced into the chamber. Once the pressure reached 100 mTorr, the oxygen plasma was excited with 13.56 MHz rf-excitation applied to a helical copper coil wrapped around a 32 mm diameter quartz tube. The $O_2$ flow rate was sustained at 35 sccm, and the rf-power was maintained at 200 W. Subsequently, $N_2$ gas was used to purge the chamber again and prepare the chamber for the next cycle of growth. The precursors used for $Al_2O_3$ and $HfO_2$ growth were dimethylaluminum isopropoxide (DMAI) and tetrakis(ethylmethylamido)hafnium (TEMAH), respectively. The bubbler temperature was set to 80 °C for DMAI and 48 °C for TEMAH, and the substrate temperature was maintained at 140 °C during growth. The lines between the bubbler and the chamber were heated ~20 °C higher than the relevant bubbler temperature and the chamber was heated to 100 °C to prevent precursor condensation. The growth rate was ~0.9 Å/cycle and ~0.7 Å/cycle for $Al_2O_3$ and $HfO_2$, respectively; the number of cycles was adjusted to deposit ~1 nm thin films on the GaN substrate. For the $HfO_2$/$Al_2O_3$/GaN stack structure, 1 nm $Al_2O_3$ was deposited on GaN and subsequently annealed in vacuum at 650 °C, and then, 2 nm $HfO_2$ was grown over the $Al_2O_3$ layer.

### C. Ultraviolet photoemission spectroscopy characterization

Ultraviolet photoemission spectroscopy (UPS) was used immediately following the ALD growth. The chamber base

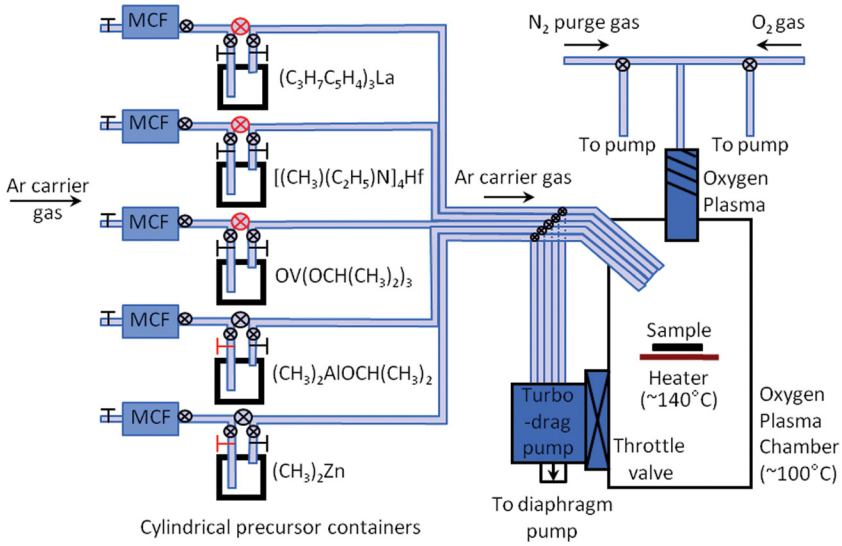


FIG. 1. Schematic illustration of the PEALD system.

pressure was $8 \times 10^{-10}$ Torr and He I, 21.2 eV radiation, was generated from research grade He gas using an UV lamp with an applied voltage of 1 kV and discharge current of 20 mA. The emitted electrons were dispersed with a VSW 50 mm hemispherical analyzer operated at a resolution of ~0.15 eV. Additionally, a negative 8 V bias was used to overcome the work function of the analyzer (4.4 eV). The system was set to scan kinetic energy from 26 to 4 eV with 0.1 eV steps to obtain the valence band spectrum of the sample, which provided the electron affinity and valence band maximum (VBM) of the film. The valence band maximum is determined by the energy difference between the Fermi level and the low binding energy cut-off of the UPS spectra, and the electron affinity is calculated by $\chi = h\nu\text{-W-}E_g$, where $h\nu$ is the ultraviolet photon energy (21.2 eV), W is the spectrum width between low and high binding energy cutoffs of the UPS spectra, and $E_g$ is the band gap of the thin film.

### D. X-ray photoemission spectroscopy characterization

*In-situ* x-ray photoemission spectroscopy (XPS) was used between various stages of the experimental process to characterize the energy core levels of the samples' constituent elements. To investigate the cleaning processes used to treat the GaN wafers, XPS spectra of the C 1s and O 1s peaks were measured at a base pressure of $8 \times 10^{-10}$ Torr. These spectra were used to determine the residual oxygen and carbon after various cleaning processes. To investigate the deposited films, XPS was utilized to measure the Ga 3d, Ga 3p, N 1s, O 1s, Al 2p, and Hf 4f core level spectra after each of the following steps: the standard cleaning process, high-k dielectric thin-film growth, 30 min annealing at 650 °C in vacuum, 5 min room temperature oxygen plasma treatment at 100 W, and finally, 30 min vacuum annealing at 650 °C. Note that throughout this process the sample was maintained in the UHV system. Mg Kα (= 1253.6 eV) x-ray radiation was used as a source, except when scanning C 1s peak since the Ga LMM lines and C 1s peak overlap. Therefore, Al Kα (= 1486.6 eV) x-rays were used to scan the C 1s peak. The x-ray source used a 4.4 A filament current, 16 mA emission current, and 13 kV accelerating voltage. The survey scans were repeated 30-80 times with a pass energy of 20 eV. The spectra were dispersed with a Fisons Clam II hemispherical analyzer with a resolution of ~1.0 eV. Through curve fitting of the core level peaks, the peak positions could be resolved to ±0.1 eV. These peak positions were then used to determine the valence band offsets.

Waldrop, Grant,[30] and Kraut *et al.*[31] give the method to calculate band offsets, which is based on the following relation:

$$\Delta E_V = (E_{CL} - E_V)_{GaN} - (E_{CL} - E_V)_{high\text{-}k\ oxide} + \Delta E_{CL}, \quad (1)$$

where $E_V$ represents the binding energy of the VBM, and $E_{CL}$ is the binding energy of the core levels. In this analysis, $\Delta E_{CL}$ is correspondingly the binding energy difference of the core levels of the GaN substrate and high-k oxide film; $(E_{CL} - E_V)_{GaN}$ and $(E_{CL} - E_V)_{high\text{-}k\ oxide}$ are the binding energy differences of the core level of Ga in GaN and the metal element in the high-k oxide with respect to its own VBM. These $(E_{CL} - E_V)$ values are essentially independent of band bending, because the valence band maximum and core level bands would be affected equally. Once these values are measured, the VBO can be calculated using only the XPS core level difference of the dielectric and semiconductor. In this study, the value of $(E_{CL} - E_V)_{high\text{-}k\ oxide}$ is calculated from the VBM value from UPS and Hf or Al core level binding energy value from XPS, immediately after deposition. Because the surface of GaN is oxygen terminated, the valence band maximum of GaN is not measured directly. According to the electronic-state studies of GaN,[8,30,32] the Ga 3d core level is 17.7-17.8 eV below the valence band maximum, and 17.8 eV is adopted in this study as the value of $(E_{CL} - E_V)_{GaN}$. Accordingly, the evolution of the XPS core levels reflects the core level differences and can be used to determine the VBO and the band alignment at the interface.

## III. RESULTS

Using this method and the relationship between the energy bands and core levels, the band bending and alignment were calculated from the XPS and UPS data for four different samples: cleaned GaN, $Al_2O_3$/GaN, $HfO_2$/GaN, and $HfO_2/Al_2O_3$/GaN stacked structure.

### A. Clean GaN

In the case of the cleaned oxygen-terminated GaN wafer, the band bending is dependent on surface contamination, which can significantly affect device performance. The contaminants on the material's surface, include absorbed molecules, organic contaminants, and native oxides. The goal in this study is to remove the carbon on the GaN surface but retain oxygen termination. This results in an oxygen-terminated surface. The oxygen contamination can be removed with high-temperature annealing ~900 °C; however, at temperatures above ~800 °C, Ga evaporation begins to occur leaving dangling bonds and increasing the surface defect concentration, which in turn increases the interfacial defect concentration.[27,28] Leaving the surface oxygen-terminated can therefore reduce the defects between high-k oxides and GaN. Fig. 2 displays the XPS of the C 1s core level from the GaN surface after various treatments, including (a) wet chemical (acetone and methanol) cleaning, (b) wet chemical (acetone, methanol, HCl) and 400 °C annealing, (c) wet chemical (acetone, methanol, HCl) and 400 °C $N_2$ plasma annealing, (d) wet chemical (acetone, methanol, HCl) and 400 °C $H_2/N_2$ plasma annealing, (e) wet chemical (acetone, methanol, HCl) and room temperature $H_2/N_2$ plasma annealing, (f) wet chemical (acetone, methanol) and 400 °C $H_2/N_2$ plasma annealing, (g) wet chemical (acetone, methanol, HCl), UV/$O_3$ and 400 °C $H_2/N_2$ plasma annealing, and (h) wet chemical (acetone, methanol, HCl) and 650 °C $H_2/N_2$ plasma annealing. In summary, the basic *ex-situ* clean involved acetone and methanol cleaning; however, this process left significant carbon contamination on the surface. This contamination was decreased with the various *in-situ*

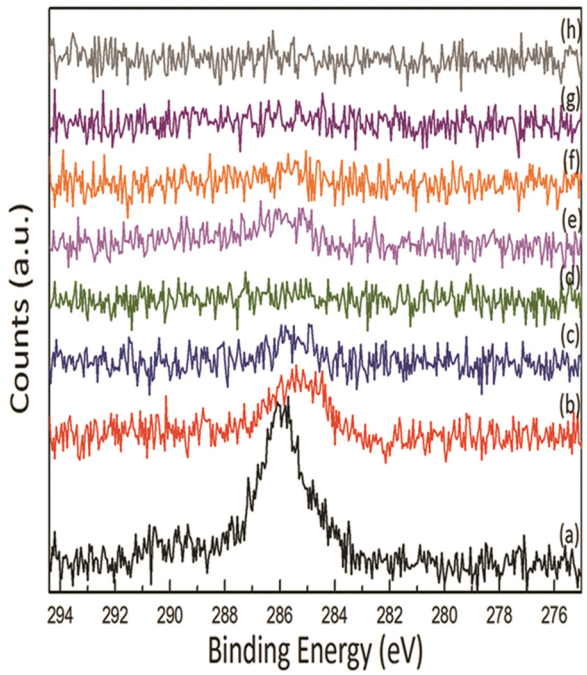


FIG. 2. XPS spectra of C 1s core level from $5 \pm 1\ \mu$m n-type Ga-face GaN treated with (a) acetone and methanol; (b) acetone, methanol, HCl, and 400 °C annealing; (c) acetone, methanol, HCl, and 400 °C $N_2$ plasma annealing; (d) acetone, methanol, HCl, and 400 °C $H_2/N_2$ plasma annealing; (e) acetone, methanol, HCl, and room temperature $H_2/N_2$ plasma annealing; (f) acetone, methanol, and 400 °C $H_2/N_2$ plasma annealing; (g) acetone, methanol, HCl, UV/$O_3$, and 400 °C $H_2/N_2$ plasma annealing; and (h) acetone, methanol, HCl, and 650 °C $H_2/N_2$ plasma annealing.

cleaning processes, where the 400 °C $H_2/N_2$ plasma process resulted in the least amount of carbon contamination. Using these two treatments as a baseline, the effects of HCl, UV/$O_3$, and higher temperature annealing were also considered and resulted in similar levels of carbon and oxygen on the surface. From these results, we established our baseline cleaning process: the *ex-situ* cleaning process was sonication in an acetone, methanol, and HCl acid bath for 10 min each, and the *in-situ* cleaning process was a 15 min 650 °C $H_2/N_2$ plasma process followed by an additional 30 min vacuum 650 °C annealing.

The surface band bending of the oxygen-terminated GaN is also investigated. XPS curve fitting results of the oxygen-terminated GaN surface give the binding energy of the Ga 3d peak as 21.0 eV, which—assuming $(E_{CL}\text{-}E_V)_{GaN}$ is 17.8 eV—indicates the VBM of the GaN is 3.2 eV below the Fermi level. Using 3.4 eV as the GaN band gap, after *ex-situ* and *in-situ* cleaning, the bands are bent upward by 0.1 eV, which is smaller than other groups' values of 0.3 eV–1.5 eV.[27,33–35] However, an additional 30 min of annealing at 650 °C immediately following plasma cleaning decreased the binding energy of the Ga 3d core level to 20.8 eV, which indicates 0.3 eV upward band bending. The band diagram of oxygen-terminated n-type Ga-face GaN is displayed in Fig. 3. In an attempt to remove the residual oxygen contamination, the GaN wafer was treated with 200 W $H_2/N_2$ combined plasma at ~880 °C for 30 min and an additional 1 h ~880 °C anneal. However, this treatment did not remove all the remaining oxygen. Fig. 4(a) shows the UPS spectra of

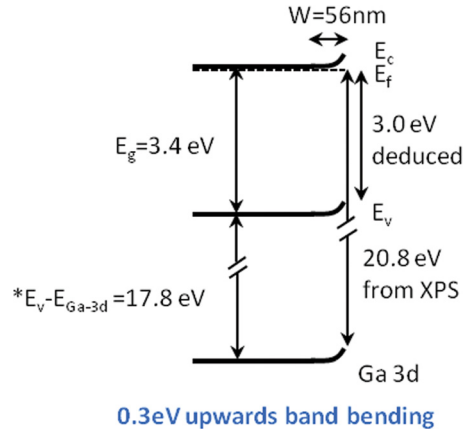


FIG. 3. Band bending diagram of an oxygen-terminated, n-type, Ga-face GaN surface.

this oxygen-terminated GaN. The VBM and the width of the spectra are 2.8 and 14.4 eV, respectively. The photo threshold energy or ionization energy of the electrons in the VBM is equal to either the energy difference between the UPS photon energy and spectra width or the sum of the electron affinity and band gap. This determines 6.8 eV as the ionization energy. Assuming 3.4 eV as the band gap, the electron affinity of oxygen-terminated GaN is 3.4 eV, which is similar to another group's value of 3.3 eV.[36] The XPS of Ga 3d is 20.4 eV below the Fermi level and therefore 17.6 eV in reference to the VBM. This is very close to the theoretical value 17.8 eV used in this paper.

### B. $Al_2O_3$/GaN

The $Al_2O_3$ film deposited on GaN was ~1 nm thick. The UPS spectra for this sample, as shown in Fig. 4(b), were used to determine the electron affinity and the VBM. It is worth mentioning here that the band gap of the amorphous $Al_2O_3$ thin film is not consistent with the bulk value of $\alpha$-$Al_2O_3$ (8.8 eV) but is dependent on the method of oxide film growth. In other words, the amorphous thin film is characterized by a lower band gap than that of the bulk.[22,23] The decrease in the band gap has been associated with defect-induced states located in the band gap.[37] In the case of $Al_2O_3$, the VBM states are associated with the O 2p states, and the CBM states are associated with the Al 3s, 3p states.[38] Rehybridization between Al 3s, 3p, and O 2p, modifies the charge transfer between Al and O, and consequently decreases the band gap. A similar study investigated amorphous $Al_2O_3$ model structures by first-principles calculations and showed that the smaller band gap could be due to the lower coordination numbers of the Al atoms in amorphous $Al_2O_3$ in comparison to those in crystalline $\alpha$-$Al_2O_3$.[39] For ALD grown $Al_2O_3$ thin films, the measured band gap is ~6.5 eV.[40–42]

The XPS core level curve fitting results of Ga 3d, Ga $3p_{3/2}$, N 1s, O 1s, and Al 2p are summarized in Table I. The results indicate the band bending development during the experimental process. After each annealing, the Ga and Al core levels shift to high binding energies by ~0.6 eV. After oxygen plasma treatment of the thin films, the core levels shift back to almost the original position measured before

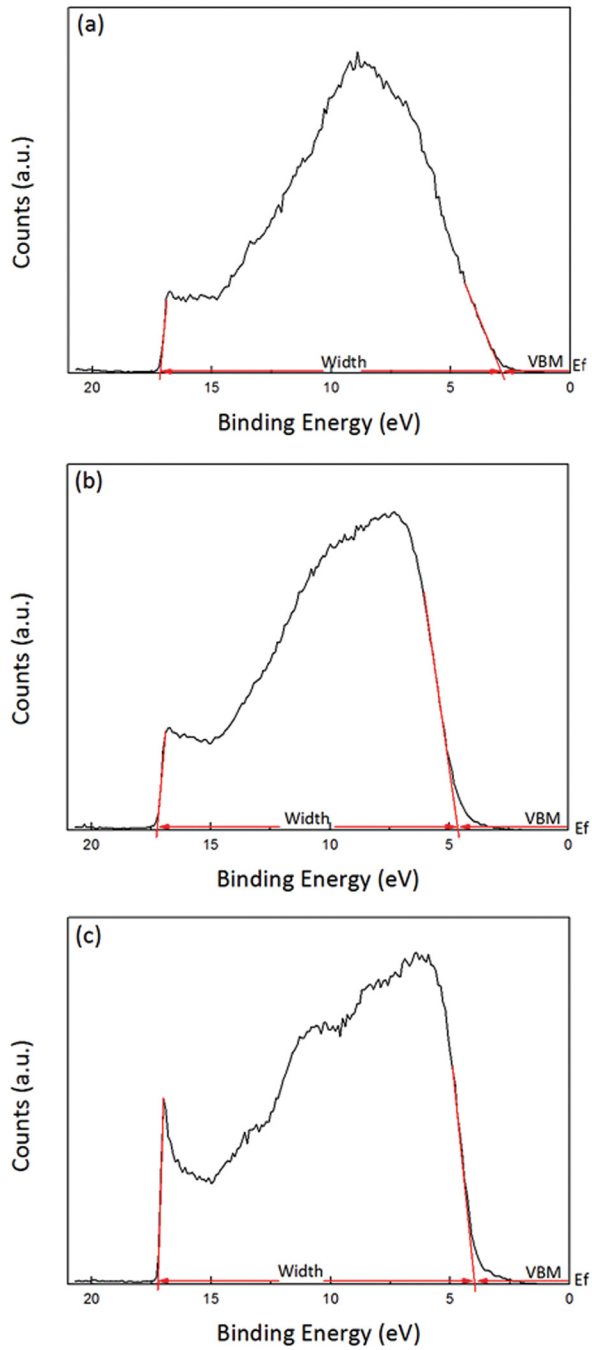


FIG. 4. UPS spectra of (a) oxygen-terminated n-type Ga-face GaN, (b) 1 nm as-deposited $Al_2O_3$ on n-type, Ga-face GaN, (c) 1 nm as-deposited $HfO_2$ on n-type, Ga-face GaN, giving the electron affinity and VBM. The valence band maximum (VBM) is the difference between the Fermi level and the low-binding energy cutoff, and the width of the spectrum, W, is used to calculate the electron affinity of the oxide.

TABLE I. XPS fitting results for Ga 3d, Ga $3p_{3/2}$, N 1s, O 1s, and Al 2p core levels. All energies are given in eV.

| Process | Ga 3d | Ga $3p_{3/2}$ | N 1s | O 1s | Al 2p |
|---|---|---|---|---|---|
| Before growth | 20.8 | 106.0 | 398.0 | 531.7 | - |
| $Al_2O_3$ deposited | 20.3 | 105.6 | 397.5 | 530.9 | 74.9 |
| $Al_2O_3$ annealed | 20.9 | 106.2 | 398.1 | 531.5 | 75.3 |
| $O_2$ plasma | 20.3 | 105.6 | 397.6 | 531.0 | 74.7 |
| Final annealing | 20.8 | 106.1 | 398.1 | 531.5 | 75.1 |

annealing. The evolution of the Ga 3d, N 1s, O 1s, and Al 2p core levels is shown in Fig. 5. Accounting for the VBM of $Al_2O_3$, which is 4.5 eV below the Fermi level, the XPS spectrum determines the Al 2p core level as 74.9 eV below the Fermi level or 70.4 eV below the VBM. The binding energy difference of the Ga 3d and Al 2p core levels peaks is measured as 54.6 eV. According to Eq. (1), the VBO of the GaN substrate and as-deposited $Al_2O_3$ film is 2.0 eV. Considering the 6.5 eV band gap of amorphous $Al_2O_3$, the corresponding conduction band offset is 1.1 eV. After annealing, the core level difference between the Ga 3d and Al 2p peaks changes slightly to 54.4 eV, which decreases the VBO to 1.8 eV. Furthermore, the core level difference is unaltered by the oxygen plasma treatment, and thus, the VBO and CBO values are equivalent to that of the annealed sample. For the final annealing step, $\Delta E_{CL}$ changes to 54.3 eV, which indicates a 1.7 eV VBO and 1.4 eV CBO. Fig. 6 shows the deduced band alignment diagrams of $Al_2O_3$ on n-type, Ga-face GaN. This figure demonstrates that although annealing and $O_2$ plasma treatment can change the screening of the polarization surface bound charge and alter the band bending conditions, the results of the band offset in this heterostructure are not significantly affected during the process steps.

In Fig. 4(b), the VBM of $Al_2O_3$ is 4.6 eV below the Fermi level. The width of the UPS spectrum is 12.7 eV, which indicates the photo threshold energy and electron affinity of $Al_2O_3$ on GaN are 8.5 and 2.0 eV, respectively. This electron affinity value is close to the value reported by Black *et al.*[43] The related XPS Al 2p core level changes to 75.1 eV, which indicates the Al 2p core level is 70.5 eV in reference to VBM. This result is comparable to the previous experimental value and is consistent with other reports.[22,44]

### C. $HfO_2$/GaN

Similarly, the results for $HfO_2$ are summarized in Figs. 4(c), 7, and 8. Fig. 4(c) shows the UPS spectra for as-deposited $HfO_2$ on GaN. The VBM is determined to be 4.0 eV relative to the Fermi level. The UPS spectrum width is 13.2 eV, and the band gap of $HfO_2$ is assumed to be 5.8 eV. This band gap value was established according to other groups' experimental values, which are reported as 5.6-6.0 eV.[22] So the photo threshold energy and electron affinity are calculated to be 8.0 and 2.2 eV, which is consistent with other reports.[8] These values are summarized in Table II along with the UPS results of oxygen terminated GaN and $Al_2O_3$/GaN. The Hf $4f_{7/2}$ core level is 17.7 eV, meaning 13.7 eV below VBM.

Fig. 7 displays the evolution of the Ga 3d, Hf $4f_{7/2}$, N 1s, O 1s, and Ga 3p core levels of 1 nm $HfO_2$/GaN during the various stages of the deposition process. The curve fitting results of these spectra are summarized in Table III. Before growth, the Ga 3d core level is 20.8 eV, which indicates 0.3 eV upward band bending at the surface. After the growth of 1 nm $HfO_2$ on GaN, the upward band bending of GaN increased by 0.5 eV. These results are similar to $Al_2O_3$ deposited on GaN. The Hf $4f_{7/2}$ core level changed to 17.5 eV, and the VBM determined from UPS shifted to 3.9 eV, which indicates the value of $(E_{CL} - E_V)_{HfO2}$ is 13.6 eV. This value

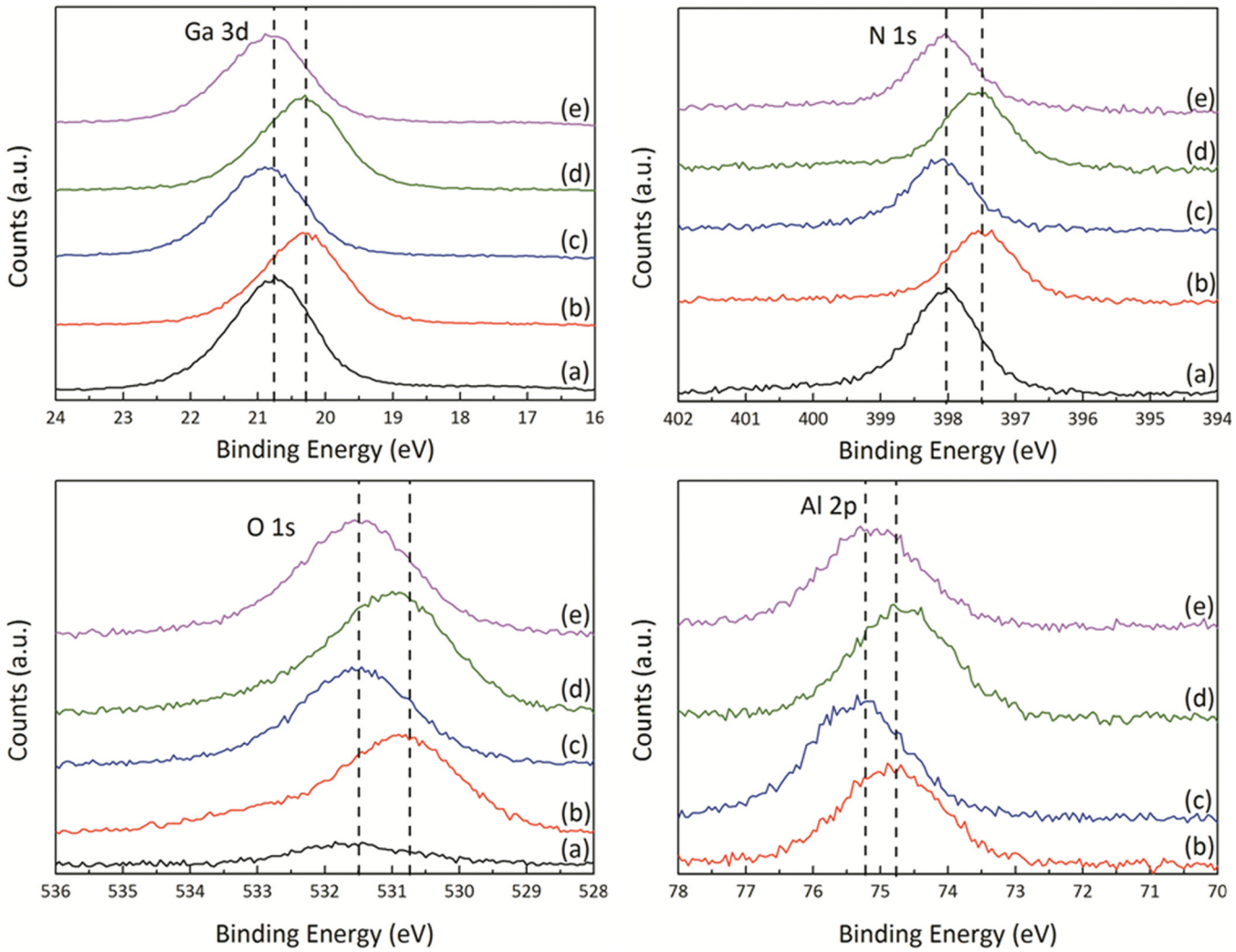


FIG. 5. Ga 3d, N 1s, O 1s, and Al 2p XPS spectra for (a) oxygen-terminated GaN, (b) 1 nm $Al_2O_3$ as deposited, (c) 1 nm $Al_2O_3$ annealed, (d) oxygen plasma treated, (e) final annealing. The initial and final states of the core level peaks after $Al_2O_3$ growth are indicated with dashed lines.

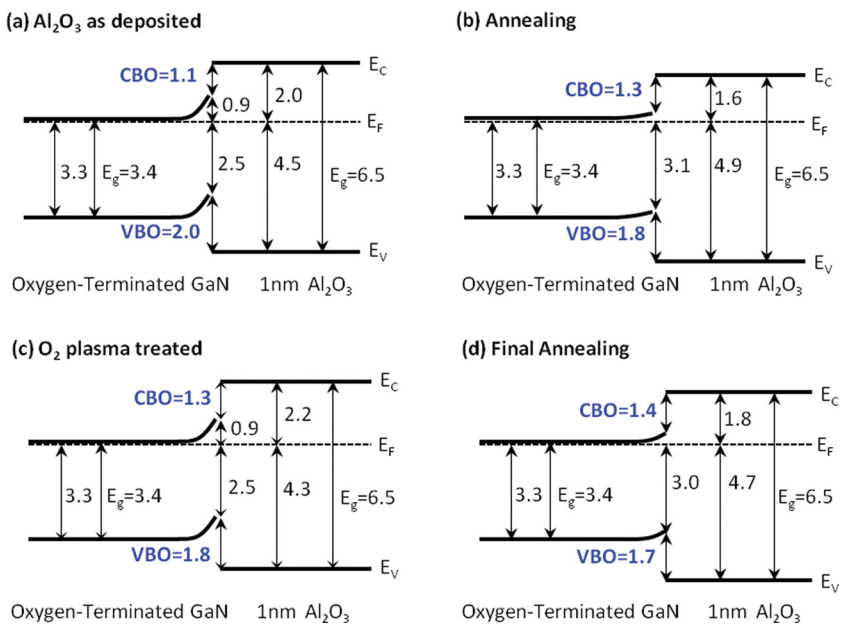


FIG. 6. Deduced band alignment diagrams for $Al_2O_3$/GaN interface (a) as deposited, (b) after annealing, (c) $O_2$ plasma treated, and (d) final annealing, where all energies are given in eV.

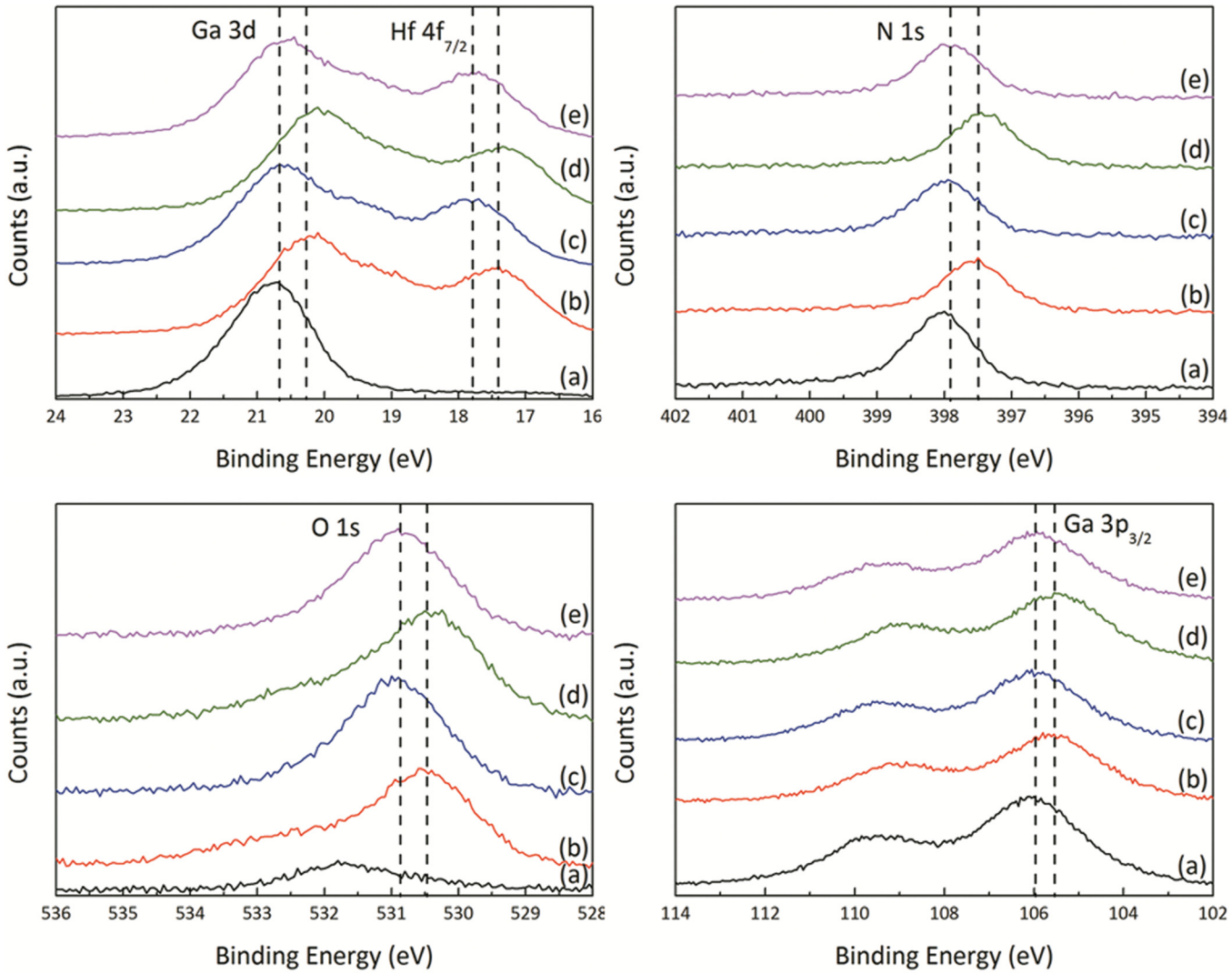


FIG. 7. Ga 3d and Hf 4f, N1s, O 1s, and Ga 3p XPS spectra for (a) oxygen-terminated GaN, (b) 1 nm $HfO_2$ as deposited, (c) 1 nm $HfO_2$ annealed, (d) oxygen plasma treated, (e) final annealing. The initial and final positions of the core level peak after $HfO_2$ growth are indicated with dashed lines.

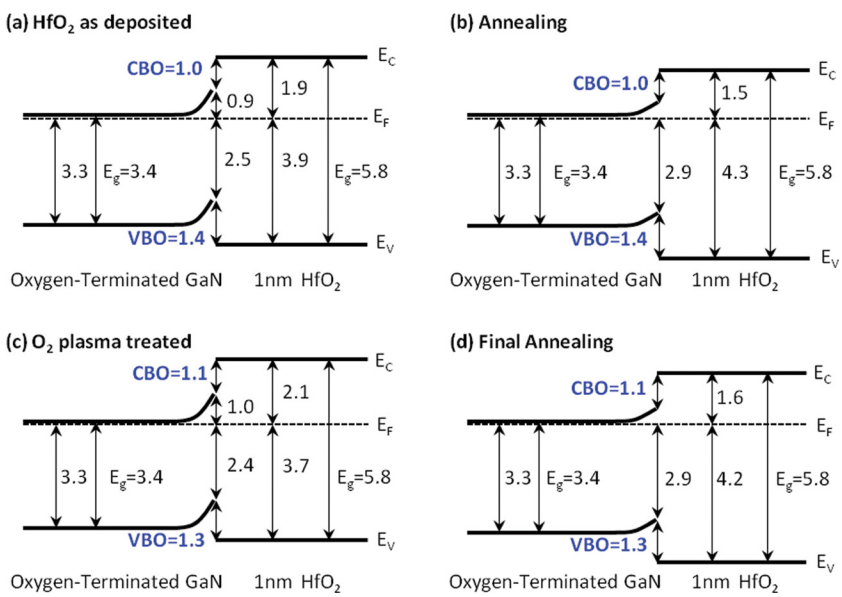


FIG. 8. Deduced band alignment diagram for $HfO_2$/GaN interface (a) as deposited, (b) after annealing, (c) $O_2$ plasma cleaning, and (d) final annealing, where all energies are given in eV.

TABLE II. UPS results of oxygen terminated GaN, as-grown $Al_2O_3$/GaN and as grown $HfO_2$/GaN. All energies are given in eV.

| | Oxygen-terminated GaN | As grown $Al_2O_3$/GaN | As grown $HfO_2$/GaN |
|---|---|---|---|
| VBM | 2.8 | 4.6 | 4.0 |
| Spectral width | 14.4 | 12.7 | 13.2 |
| Photo threshold energy | 6.8 | 8.5 | 8.0 |
| Band gap | 3.4 | 6.5 | 5.8 |
| Electron affinity | 3.4 | 2.0 | 2.2 |

is consistently repeatable and agrees with a prior report.[45] The core level difference between Hf $4f_{7/2}$ and Ga 3d is −2.8 eV. Hence, the VBO of the as-deposited $HfO_2$/GaN heterostructure is 1.4 eV. Accounting for the 5.8 eV band gap of the $HfO_2$ thin film, the corresponding CBO is 1.0 eV. The annealing and oxygen plasma treatment following the growth shift the bands by almost the same values, and therefore the VBO and CBO are still ∼1.4 and ∼1.0 eV, respectively. Fig. 8 shows the deduced band alignment of $HfO_2$ on Ga face GaN for different experimental processing.

These values are different from previous $HfO_2$/GaN band offsets reported by Cook *et al.*,[8] which give −0.1 and 0.3 eV as the VBO for as-grown and annealed $HfO_2$/n-type, Ga-face GaN, respectively. (We note that the same photoemission systems were employed in both the prior and current study.) Further investigation reveals this difference stems from an ∼0.5 eV difference in the Hf $4f_{7/2}$ core level with respect to the Ga 3d core level and the energy separation between Hf $4f_{7/2}$ and VBM; these discrepancies culminate ∼1 eV difference in the VBOs. This disparity is likely the result of the different cleaning and deposition processes. In the previous work, the GaN was annealed in ammonia at a higher temperature to remove any oxygen from the surface, while this research retained oxygen termination on the GaN after cleaning, leaving an interstitial oxygen layer at the interface. The interlayer changes the electronegativity of the surface atoms and thus the interfacial dipole and subsequent electronic properties. Furthermore, in the previous study, the films were grown in 4 Å increments of MBD Hf followed by oxygen plasma; this suggests that the film may have a different structure than the films grown by PEALD. The dissimilar structure would explain the difference between the VBM and the Hf $4f_{7/2}$ core level as well as the shift in the Hf 4f core levels, while the O 1s and Ga core levels remain comparable.

TABLE III. XPS peak fitting results for Ga 3 d, Ga $3p_{3/2}$, N 1s, O1s, and Hf $4f_{7/2}$ core levels. All energies are given in eV.

| Process | Ga 3d | Ga $3p_{3/2}$ | N 1s | O 1s | Hf $4f_{7/2}$ |
|---|---|---|---|---|---|
| Before growth | 20.8 | 106.1 | 398.0 | 531.7 | - |
| $HfO_2$ deposited | 20.3 | 105.6 | 397.6 | 530.4 | 17.5 |
| $HfO_2$ annealed | 20.7 | 106.0 | 398.0 | 530.9 | 17.9 |
| $O_2$ plasma | 20.2 | 105.5 | 397.4 | 530.4 | 17.3 |
| Final annealing | 20.7 | 106.0 | 397.9 | 530.9 | 17.8 |

TABLE IV. XPS peak fitting results for Ga 3d, Ga $3p_{3/2}$, N 1s, O 1s, Al 2p, and Hf $4f_{7/2}$ core levels in eV. The bracketed values were modified according to the fixed core level difference between Ga 3d and Ga $3p_{3/2}$.

| Process | Ga 3d | Ga $3p_{3/2}$ | N 1s | O 1s | Al 2p | Hf $4f_{7/2}$ |
|---|---|---|---|---|---|---|
| $HfO_2$ deposited | 20.0 (20.3) | 105.6 | 397.6 | 530.5 | 74.4 | 17.2 |
| $HfO_2$ annealed | 20.4 (20.6) | 105.9 | 397.9 | 530.7 | 74.9 | 17.7 |
| $O_2$ plasma | 20.1 (20.3) | 105.6 | 397.5 | 530.3 | 74.4 | 17.3 |
| Final annealing | 20.3 (20.7) | 106.0 | 397.9 | 530.7 | 74.9 | 17.8 |

### D. $HfO_2/Al_2O_3$/GaN

The XPS core-level peak-fitting results for the stacked structures are shown in Table IV for the Ga 3d, Ga $3p_{3/2}$, N 1s, O 1s, Al 2p, and Hf $4f_{7/2}$ peaks. These results are used to develop the band alignment diagrams for the stacked structure, which consists of 2 nm $HfO_2$ on 1 nm $Al_2O_3$ on an n-type Ga-face GaN wafer. Fig. 9 illustrates the evolution of the XPS core level spectra. The values of $(E_{CL} - E_V)_{GaN}$, $(E_{CL} - E_V)_{Al_2O_3}$, and $(E_{CL} - E_V)_{HfO_2}$ are fixed at 17.8, 70.4, and 13.6 eV, respectively. Assuming the charges are distributed only at the interfaces, the constructed bands of $HfO_2$ are flat and $Al_2O_3$ are inclined indicating the presence of an electric field. Furthermore, the valence band offset of $Al_2O_3$ with respect to GaN is assumed to be 1.8 eV, unchanged from previous results.

From the fixed VBO of $Al_2O_3$/GaN and shift of GaN core levels, the core level values of $Al_2O_3$ at the $Al_2O_3$/GaN interface can be established. The XPS core level value of the Al 2p peak represents the average binding energy of the Al 2p core level in the interfacial layer, which can be used to determine the binding energy of Al 2p core level in the middle of the $Al_2O_3$ interfacial layer, and the core level of the Al 2p at the $HfO_2/Al_2O_3$ interface can be ascertained from the inclined band property. After $HfO_2$ is grown on $Al_2O_3$, the Ga 3d peak should shift to 20.3 eV rather than 20.0 eV, because the energy difference between the Ga $3p_{3/2}$ and 3d core levels was 85.3 eV. After $HfO_2$ growth, the prominent Hf $4f_{5/2}$ peak overlaps with the Ga 3d peak, which obscures the Ga 3d peak fit. The measured values for the Ga 3d core levels are, therefore, modified using the Ga $3p_{3/2}$ core level results. (These values are bracketed in Table IV.) The modified Ga 3d peak value (20.3 eV) is then used to determine the VBM of GaN; accounting for $(E_{CL} - E_V)_{GaN} = 17.8$ eV, the VBM of GaN is 2.5 eV below the Fermi level. Assuming the VBO at the $Al_2O_3$/GaN interface is 1.8 eV, the VBM of $Al_2O_3$ at the $Al_2O_3$/GaN interface is thus 4.3 eV below the Fermi level. According to the curve fitting value of the Al 2 p core level, the VBM in the middle of the $Al_2O_3$ film is 4.0 eV below the Fermi level. This value indicates the potential drop across the $Al_2O_3$ film is 0.6 eV, and the VBM of $Al_2O_3$ at the $HfO_2/Al_2O_3$ heterostructure is 3.7 eV. The VBM of $HfO_2$ is 3.6 eV below the Fermi level, which is determined from the XPS core level value of the Hf $4f_{7/2}$ peak. Therefore, the VBO and CBO at the $HfO_2$/$Al_2O_3$ interface are 0.1 and 0.6 eV, respectively. Furthermore, the VBO and CBO between GaN and $HfO_2$ are 1.1 and 1.3 eV, respectively. After annealing, the Ga $3p_{3/2}$ and Al 2p core levels move to higher binding energy by 0.3 and 0.5 eV,

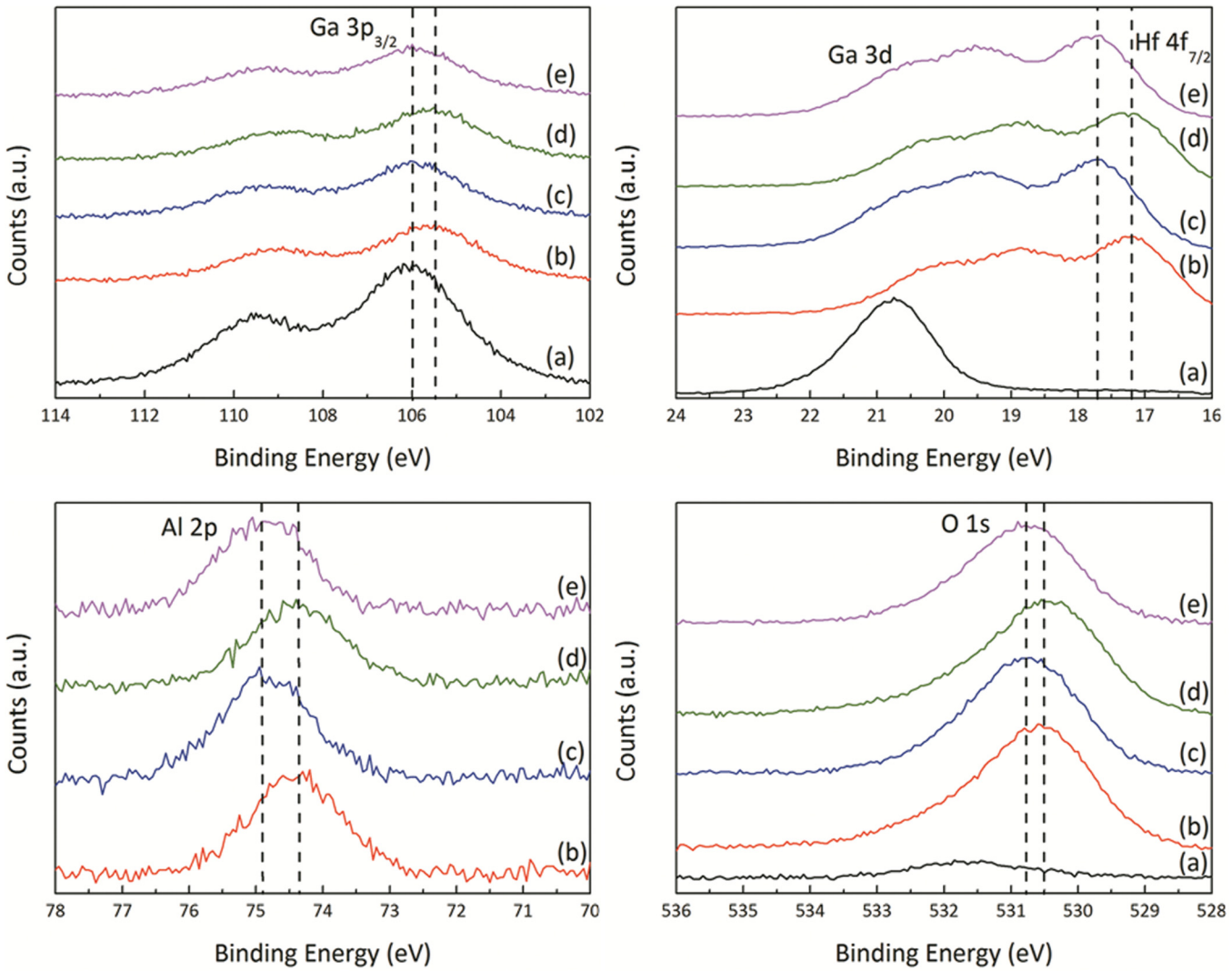


FIG. 9. Ga 3p, Ga 3d and Hf 4f, Al 2p, and O 1s XPS core level spectra for (a) before growth, (b) $HfO_2/Al_2O_3$/GaN as deposited, (c) $HfO_2/Al_2O_3$/GaN annealed, (d) oxygen plasma treated, and (e) final annealing.

respectively, indicating a decrease of the potential drop across the $Al_2O_3$ film and the charge accumulation at the $HfO_2/Al_2O_3$ interface. The band bending diagrams of the stacked structure are depicted in Fig. 10, and the results of the VBO and CBO of the various interfaces in the stacked structure are summarized in Table V, where the band relations of $HfO_2$/GaN include the electric field in the dielectric. As suggested, the $Al_2O_3$ passivation layer provides enhanced thermodynamic stability and a sufficient valence band and conduction band barrier height (more than 1.3 eV), which may improve the performance and decrease the leakage current of $HfO_2$/GaN structures.

## IV. DISCUSSION

As previously mentioned, the interface band alignment of two materials reveals the confinement characteristics of carriers. Therefore, understanding the properties that influence band alignment can illuminate critical aspects of carrier behavior that may affect device performance and reliability. Consequently, there are several approaches, which attempt to explain the band bending and alignment; this includes the polarization, which determines the band bending of the bare wafer as well as the electron affinity and charge neutrality level models, which provide theoretical band alignments for dielectric/semiconductor interfaces. These models are discussed in this section in addition to the high temperature annealing and various plasma treatments used throughout the experiment.

### A. Polarization of GaN

Wurtzite GaN exhibits a large spontaneous polarization and piezoelectric polarization ($P_{SP}$ and $P_{PE}$),[46,47] which leads to band bending at the surface. The spontaneous polarization of Ga-face GaN ($P_{SP} = 0.033\ C/m^2$)[48] points from the surface to the bulk. The piezoelectric polarization, on the other hand, is negligible in comparison. The polarization produces a negative bound surface charge at the Ga face and positive bound charge at the N face on the order of $\sim 2.1 \times 10^{13}$ charges/cm$^2$. The positive bound charge may be screened by free electrons, while the negative bound sheet charge is partially compensated by the positive ionized donors. If the negative bound sheet charge is completely compensated by the

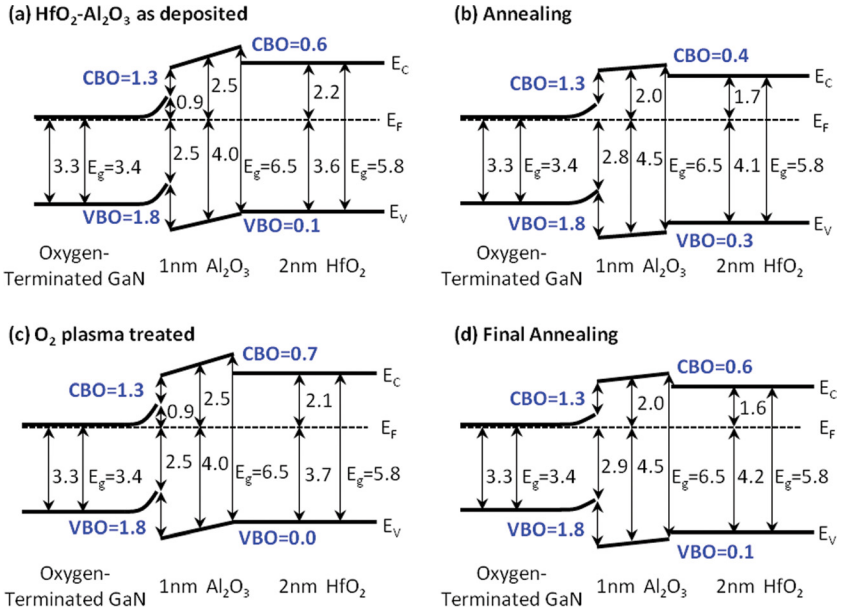


FIG. 10. Band alignment diagram for $HfO_2/Al_2O_3/GaN$ interface (a) as deposited, (b) after annealing, (c) after oxygen plasma, and (d) after second annealing, where all energies are given in eV.

positive ionized donors, the thickness of the space charge region is equal to the bound sheet charge density ($=2.1 \times 10^{13}$ charges/cm$^2$) divided by the doping concentration ($N_D = 1 \times 10^{17}$ cm$^{-3}$), which is 2.1 $\mu$m. Then, the surface potential $\Phi_S$ can be calculated by the following relation:

$$\Phi_S = -\frac{qN_D}{2\varepsilon\varepsilon_o} W^2, \tag{2}$$

where W is the depletion layer thickness, and $\varepsilon(=9.5)$ is the dielectric constant of GaN. This calculation gives a surface potential of $-420$ V and an average electric field of 200 MV/m, which would be represented as 420 eV upward band bending at the GaN surface. In equilibrium, the large field will lead to inversion, which limits the band bending to the band gap value of the material, 3.4 eV in this case. This analysis indicates the polarization bound charge cannot only be completely compensated by the positive ionized donors. The experimental upward band bending for Ga-face GaN is typically reported to be between 0.3 and 1.5 eV,[18,25,26] well below the band gap value. This indicates that the surface is heavily compensated. In order to achieve the experimental band bending, the space charge region width and the area density of the ionized donors can be only between 56-126 nm and $5.6 \times 10^{11}$-$1.3 \times 10^{12}$ cm$^{-2}$, respectively. So the surface would have to be screened by $\sim 2 \times 10^{13}$ charges/cm$^2$, which could include structural defects, Ga termination, surface contamination (such as absorbed oxygen atoms), surface states or absorbates causing Fermi level pinning, or additional charge compensation.[49]

TABLE V. Summary of band offset values for the $HfO_2/Al_2O_3/GaN$ structure, where all energies are given in eV. Note the band relation of $HfO_2$/GaN includes the electric field in the dielectric.

| | $Al_2O_3$-GaN | | $Al_2O_3$-$HfO_2$ | | $HfO_2$-GaN | |
|---|---|---|---|---|---|---|
| Process | VBO | CBO | VBO | CBO | VBO | CBO |
| As deposited | 1.8 | 1.3 | 0.1 | 0.6 | 1.1 | 1.3 |
| Annealed | 1.8 | 1.3 | 0.3 | 0.4 | 1.3 | 1.1 |
| Oxygen plasma treated | 1.8 | 1.3 | 0.0 | 0.7 | 1.2 | 1.2 |
| Final annealing | 1.8 | 1.3 | 0.1 | 0.6 | 1.3 | 1.1 |

### B. Oxygen coverage on GaN

After the standard cleaning process, oxygen termination was retained on the GaN surface. The oxygen coverage can be calculated from the following relation:[50]

$$\Theta_O = \frac{I_O}{I_{Ga}} * \frac{S_{Ga}}{S_O} * \sum_{n=0}^{\infty} \exp\left[\frac{-nd_{GaN}}{\lambda_{Ga}\cos[\phi]}\right], \tag{3}$$

where $\Theta_O$ is the coverage or the number of absorbed oxygen per unit area (atoms/cm$^2$) divided by the number of Ga or N atoms per unit area (atoms/cm$^2$) in the c plane. One monolayer (ML) coverage refers to one oxygen atom per surface lattice site. The $I_{Ga}$ and $I_O$ are the integrated intensities of the Ga 3d and O 1s peaks; $S_O$ is the atomic sensitivity factor for O 1s, 0.711; $\lambda_{Ga}$ is the inelastic mean free path (IMFP) of Ga 3d electrons with kinetic energies $\sim$1200 eV, which is estimated to be 24 Å;[51] $\phi$ is the angle between the normal direction and the analyzer, which is 20° for the XPS setup; and, d is the distance between two Ga planes, which is 2.6 Å. The sum of the exponential function in this relation represents the Ga 3d electrons from different Ga planes. The infinite limit can be replaced by a large number, such as 25, because the exponential function decreases rapidly with increased thickness and only surface Ga layers would contribute significantly to the sum. $S_{Ga}$ is the remaining unknown in the relation, which can be deduced from a similar equation for stoichiometric GaN

$$\frac{I_N}{I_{Ga}} = \frac{S_N * \sum_{n=0}^{\infty} \exp\left[\frac{-\left(n+\frac{1}{3}\right)d_{GaN}}{\lambda_N \cos[\phi]}\right]}{S_{Ga} * \sum_{n=0}^{\infty} \exp\left[\frac{-nd_{GaN}}{\lambda_{Ga}\cos[\phi]}\right]}, \tag{4}$$

where $S_N = 0.477$ and $\lambda_N = 18$ Å for the N 1s electrons, which has kinetic energy ~856 eV.[51] For wurtzite GaN, an N atom sits at the center of the tetrahedral structure formed by four Ga atoms. Because the first layer of Ga-face GaN would be a Ga layer, and the distance between the first Ga layer and N layer is 1/3 of d due to tetrahedral structure, the layer number, n, of nitrogen should be modified by $n + 1/3$. Combining these two relations, the oxygen coverage on GaN surface is $2.29 \pm 0.15$ ML, which would correspond to ~0.5 nm $Ga_2O_3$. However, this value is sensitive to the cleaning process; slight alterations in the sonication time of the wet chemical as well as the plasma treatment time and temperature results in oxygen coverage ranging from 2.17 to 2.50 ML. To remove the residual oxygen contamination, the GaN wafer was treated with 200 W $H_2/N_2$ combined plasma at ~880 °C for 30 min and an additional 1 h ~880 °C annealing. However, the oxygen coverage on the surface of GaN is still ~1.63 ML.

### C. Plasma treatment and annealing effects

As noted in the results, the plasma treatments altered the band bending. For example, the core levels of thin film and GaN substrate move to low binding energy by ~0.5 eV after oxygen plasma treatment. It is likely that the oxygen plasma introduces a high concentration of defects or interstitial oxygen atoms, which act as deep electron traps or double acceptors, respectively.[52] These defects are compensated by ionized donors in the GaN and widen the depletion region, which increases the upward band bending. High temperature annealing can remove the defects or excess interstitial oxygen from the film and subsequently reduce the upward band bending. Consequently, the core levels shift back to higher binding energy, which is confirmed by the results. Mixed hydrogen and nitrogen treatments, on the other hand, may induce donor-like defects, which similarly cause downward band bending that can be reversed with annealing.

### D. Band alignment models for $Al_2O_3$/GaN and $HfO_2$/GaN

Modeling of semiconductor interfaces has been of interest since Schottky and Mott independently introduced their theories in 1938.[53] However, despite this relatively long history, it is still subject to some debate. Presently, there are two common adaptations of interface modeling, which argue for a different point of alignment at the interface. In this paper, we identify these as the electron affinity model and the charge neutrality level model.

The electron affinity (EA) model, presented by Anderson,[54] is based on the assumption that the vacuum levels of the two materials align at the interface. This premise can be extended to the semiconductor-semiconductor interface, or more specifically the high-k oxide/GaN interfaces. Considering the vacuum-level alignment, the VBO

$$\begin{aligned}\Delta E_V &= (E_{g,GaN} + \chi_{GaN}) - (E_{g,\text{high-k oxide}} + \chi_{\text{high-k oxide}}) \\ &= I_{GaN} - I_{\text{high-k oxide}},\end{aligned} \tag{5}$$

where $E_g$ and $\chi$ are the band gap and the electron affinity of the given semiconductor, respectively. The sum of these two values will give the photo threshold energy, $I$. For oxygen-terminated GaN, $Al_2O_3$, and $HfO_2$, the photo threshold energies are 6.8, 8.5, and 8.0 eV, respectively. The calculated VBOs of the $Al_2O_3$/GaN and $HfO_2$/GaN heterostructures are thus 1.7 and 1.2 eV, which are similar to the experimental values of 1.8 and 1.4 eV. However, the similarity in these values is potentially misleading as the model represents an idealized case that is not often physically realized. More explicitly, the EA model assumes no charge transfer at the interface.

An alternative model, first proposed by Tejedor and Flores[55] and later calculated by Tersoff,[56] evaluates the available states at the interface. This model assumes the wave function of electrons in the metal decays exponentially across the interface and induces states in the gap. These gap states behave donor-like closer to the valence band and acceptor-like closer to the conduction band. The point where the contribution from both the acceptor- and donor-like states are equal is the branch point energy or charge neutrality level (CNL). The CNL then becomes the point of alignment at the heterostructure, assuming that there is some charge transfer, which creates an interfacial dipole. This model was further adapted to account for Fermi pinning at the interface,[57] by considering the pining factor, S. This was empirically demonstrated[58,59] to obey the following relation:

$$S = \frac{1}{1 + 0.1(\varepsilon_\infty - 1)^2}, \tag{6}$$

where $\varepsilon_\infty$ is the optical dielectric constant of the material. This modifies the alignment of the energy levels at the interface, where the VBO is given by the following relation:

$$\begin{aligned}\Delta E_V = {} & E_{CNL,\text{high-k oxide}} - E_{CNL,GaN} \\ & - S[I_{GaN} - I_{\text{high-k oxide}} \\ & - (E_{CNL,GaN} - E_{CNL,\text{high-k oxide}})],\end{aligned} \tag{7}$$

where $E_{CNL,GaN}$ and $E_{CNL,\text{high-k oxide}}$ are the charge neutrality levels of the semiconductor and oxide measured from VBM. When the CNLs of the materials are aligned, the calculation is modified by the dimensionless S factor of the wider band gap material, which accounts for Schottky pinning. In the Schottky limit of no pinning ($S = 1$), there is no charge transfer, and the electron affinity model determines the VBO. In the limit of strong pinning ($S = 0$), the semiconductors are aligned at the CNL. For $Al_2O_3$ and $HfO_2$, the S factors are 0.69 and 0.53, respectively.[36] The CNLs of GaN, $Al_2O_3$, and $HfO_2$ calculated by local density approximation (LDA) are 2.3, 3.9, and 3.7 eV[60,61] with respect to VBM. These CNLs determine the VBOs at the $Al_2O_3$/GaN and $HfO_2$/GaN interfaces as 1.7 and 1.3 eV, very close to the experimentally measured values. On the other hand, the empirically determined CNLs of GaN, $Al_2O_3$, and $HfO_2$, 2.3, 3.0, and 2.3 eV, vary from the theoretical values.[60] Using the empirical values, the VBOs at the $Al_2O_3$/GaN and $HfO_2$/GaN interfaces are 1.4 and 0.6 eV, significantly smaller than the experimentally determined values of this report.

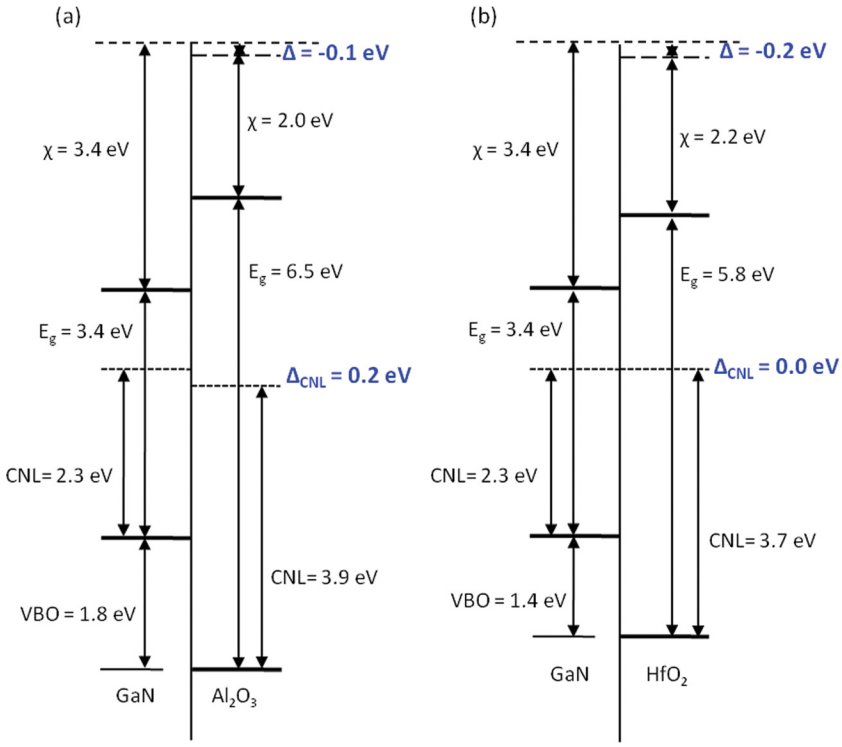


FIG. 11. Band alignment diagram for $Al_2O_3$/GaN (a) and $HfO_2$/GaN (b) interfaces. The dashed line at the top of the figure corresponds to the electron affinity of GaN. The deviation from the electron affinity model is shown as Δ, and the deviation from the charge neutrality level model in the limit of strong pinning, S = 0, is marked as $\Delta_{CNL}$. The VBO was measured experimentally, and the charge neutrality levels of GaN, $HfO_2$, and $Al_2O_3$ were provided by theoretical calculations.[36,61]

There is an additional factor to consider when evaluating the consistency of these models. Several researchers[62–65] have shown that the electron affinity of a material is dependent on the electronegativity of the adsorbed atoms. In other words, the electron affinity of the clean surface, which was used in the above calculations, is not necessarily an accurate representation of the electron affinity of that material at an interface. Investigation of the electronegativities of the elements involved suggests that the electron affinity of the high-k oxide will increase and/or the GaN substrate will decrease. Either of these changes will increase the valence band offsets determined by both models. Since both models report values lower than the experimentally determined VBOs, this correction further supports the experimentally determined VBOs.

In an attempt to better understand the similarity of these two models, the above calculations are considered in Fig. 11. The slight disparities of the charge neutrality levels and electron affinity levels are marked as $\Delta_{CNL}$ and Δ. These can be explained in terms of experimental error, inaccurate determination of the electron affinities, and Schottky pinning, which is not accounted for in this figure and will contribute to $\Delta_{CNL}$.

## V. CONCLUSION

The band alignments of high-k gate oxides $Al_2O_3$ and $HfO_2$ as well as the stacked structure $HfO_2/Al_2O_3$ on n-type Ga-face GaN have been investigated. An *ex-situ* wet chemical clean with acetone, methanol, and HCl and an *in-situ* clean with 15 minute $H_2/N_2$ plasma and additional 30 min annealing at 650 °C provided an oxygen-terminated GaN surface with 2.29 ± 0.15 ML of oxygen and 0.3 eV upward band bending. These values, while consistent with other groups' experiment data, are well below the calculation predicted from the polarization, which suggests that the surface is compensated at a level of $\sim 10^{13}$ $cm^{-2}$. The electron affinity of $Al_2O_3$ and $HfO_2$ was measured to be 2.0 and 2.2 eV, respectively. The valence band offsets at $Al_2O_3$/GaN and $HfO_2$/GaN heterostructures were 1.8 and 1.4 eV, which indicated corresponding conduction band offsets of 1.3 and 1.0 eV. These band offset values are similar to the theoretical values calculated from the electron affinity model and charge neutrality level model. Annealing and re-oxidization could change the interface charges and alter the electric field in the high-k oxide and the band bending at the GaN interface. For the $HfO_2/Al_2O_3$/GaN stacked structure, the valence band offset and conduction band offset of $HfO_2$ with respect to GaN were ~1.3 and 1.1 eV respectively, which is very close to the values in the sample $HfO_2$/GaN structure and indicates the interfacial passivation layer does not significantly alter the band offset of the $HfO_2$/GaN heterostructure.

## ACKNOWLEDGMENTS

This research was supported by the Office of Naval Research through the DEFINE MURI program, N00014-10-1-0937. We also appreciate the helpful discussions with Xin Liu and Tianyin Sun and the Rutherford Backscattering Spectrometry measurements provided by Barry Wilkens at the Center for Solid-State Science.

[1]P. D. Ye, B. Yang, K. K. Ng, J. Bude, G. D. Wilk, S. Halder, and J. C. M. Hwang, Appl. Phys. Lett. **86**, 063501 (2005).
[2]S. Ootomo, T. Hashizume, and H. Hasegawa, Phys. Status Solidi C **0**, 90 (2002).
[3]T. Hashizume, S. Ootomo, and H. Hasegawa, Appl. Phys. Lett. **83**, 2952 (2003).
[4]Y. Z. Yue, Y. Hao, Q. Feng, J. C. Zhang, X. H. Ma, and J. N. Ni, Chin. Phys. Lett. **24**, 2419 (2007).
[5]Y. Hao, Y. Z. Yue, Q. Feng, J. C. Zhang, X. H. Ma, and J. N. Ni, Chin. J. Semicond. **28**, 1674 (2007).

[6]Y. C. Chang, H. C. Chiu, Y. J. Lee, M. L. Huang, K. Y. Lee, M. Hong, Y. N. Chiu, J. Kwo, and Y. H. Wang, Appl. Phys. Lett. **90**, 232904 (2007).
[7]C. F. Shih, K. T. Hung, C. Y. Hsiao, S. C. Shu, and W. M. Li, J. Alloys Compd. **480**, 541 (2009).
[8]T. E. Cook, Jr., C. C. Fulton, W. J. Mecouch, R. F. Davis, G. Lucovsky, and R. J. Nemanich, J. Appl. Phys. **94**, 7155 (2003).
[9]Y. Dora, S. Han, D. Klenov, P. J. Hansen, K. S. No, U. K. Mishra, S. Stemmer, and J. S. Speck, J. Vac. Sci. Technol. B **24**, 575 (2006).
[10]R, Mehandru, B. Luo, J. Kim, F. Ren, B. P. Gila, A. H. Onstine, C. R. Abernathy, S. J. Pearton, D. Gotthold, R. Birkhahn, B. Peres, R. Fitch, J. Gillespie, T. Jenkins, J. Sewell, D. Via, and A. Crespo, Appl. Phys. Lett. **82**, 2530 (2003).
[11]B. Luo, J. W. Johnson, B. P. Gila, A. Onstine, C. R. Abernathy, F. Ren, S. J. Pearton A. G. Baca, A. M. Dabiran, A. M. Wowchack, and P. P. Chow, Solid-State Electron. **46**, 467 (2002).
[12]H. Cho, K. P. Lee, B. P. Gila, C. R. Abernathy, S. J. Pearton, and F. Ren, Solid-State Electron. **47**, 1757 (2003).
[13]H. Cho, K. P. Lee, B. P. Gila, C. R. Abernathy, S. J. Pearton, and F. Ren, Electrochem. Solid-State Lett. **6**, G149 (2003).
[14]J. Kim, R. Mehandru, B. Luo, F. Ren, B. P. Gila, A. H. Onstine, C. R. Abernathy, S. J. Pearton, and Y. Irokawa, Appl. Phys. Lett. **80**, 4555 (2002).
[15]B. P. Gila, A. H. Onstine, J. Kim, K. K. Allums, F. Ren, C. R. Abernathy, and S. J. Pearton, J. Vac. Sci. Technol. B **21**, 2368 (2003).
[16]B. P. Gila, J. Kim, B. Luo, A. Onstine, W. Johnson, F. Ren, C. R. Abernathy, and S. J. Pearton, Solid-State Electron. **47**, 2139 (2003).
[17]M. Hong, J. Kwo, S. N. G. Chu, J. P. Mannaerts, A. R. Kortan, H. M. Ng, A. Y. Cho, K. A. Anselm, C. M. Lee, and J. I. Chyi, J. Vac. Sci. Technol. B **20**, 1274 (2002).
[18]M. Hong, K. A. Anselm, J. Kwo, H. M. Ng, J. N. Baillargeon, A. R. Kortan, J. P. Mannaetrs, A. Y. Cho, C. M. Lee, J. I. Chyi, and T. S. Lay, J. Vac. Sci. Technol. B **18**, 1453 (2000).
[19]F. Ren, C. R. Abernathy, J. D. Mackenzie, B. P. Gila, S. J. Pearton, M. Hong, M. A. Marcus, M. J. Schurman, A. G. Baca, and R. J. Shul, Solid-State Electron. **42**, 2177 (1998).
[20]F. Ren, M. Hong, S. N. G. Chu, M. A. Marcus, M. J. Schurman, A. Baca, S. J. Pearton, and C. R. Abernathy, Appl. Phys. Lett. **73**, 3893 (1998).
[21]H. B. Profijt, S. E. Potts, M. C. M. van de Sanden, and W. M. M. Kessels, J. Vac. Sci. Technol. A **29**, 050801 (2011).
[22]E. Bersch, S. Rangan, R. A. Bartynski, E. Garfunkel, and E. Vescovo, Phys. Rev. B. **78**, 085114 (2008).
[23]V. V. Afanas'ev and A. Stesmans, J. Appl. Phys. **102**, 081301 (2007).
[24]I. Kim, J. Koo, J. Lee, and H. Jeon, Jpn. J. Appl. Phys. Part 1 **45**, 919 (2006).
[25]Y. Q. Wu, T. Shen, P. D. Ye, and G. D. Wilk, Appl. Phys. Lett, **90**, 143504 (2007).
[26]W. J. Mecouch, B. P. Wagner, Z. J. Reitmeier, R. F. Davis, C. Pandarinath, B. J. Rodriguez, and R. J. Nemanich, J. Vac. Sci. Technol. A **23**, 72 (2005).
[27]K. M. Tracy, W. J. Mecouch, R. F. Davis, and R. J. Nemanich, J. Appl. Phys. **94**, 3163 (2003).
[28]S. W. King, J. P. Barnak, M. D. Bremser, K. M. Tracy, C. Ronning, R. F. Davis, and R. J. Nemanich, J. Appl. Phys. **84**, 5248 (1998).
[29]L. L. Smith, S. W. King, R. J. Nemanich, and R. F. Davis, J. Electron. Mater. **25**, 805 (1996).
[30]J. R. Waldrop and R. W. Grant, Appl. Phys. Lett. **68**, 2879 (1996).
[31]E. A. Kraut, R. W. Grant, J. R. Waldrop, and S. P. Kowalczyk, *Heterojunction Band Discontinuities: Physics and Device Applications*, edited by F. Capasso and G. Margaritondo (Elsevier, New York, 1987).
[32]J. Hedman and N. Mårtensson, Phys. Scr. **22**, 176 (1980).
[33]P. Lorenz, T. Haensel, R. Gutt, R. J. Koch, J. A. Schaefer, and S. Krischok, Phys. Status Solidi B **247**, 1658 (2010).
[34]H. W. Jang, J. H. Lee, and J. L. Lee, Appl. Phys. Lett. **80**, 3955 (2002).
[35]C. I. Wu, A. Kahn, N. Taskar, D. Dorman, and D. Gallagher, J. Appl. Phys. **83**, 4249 (1998).
[36]J. Robertson and B. Falabretti, J. Appl. Phys. **100**, 014111 (2006).
[37]I. Costina and R. Franchy, Appl. Phys. Lett. **78**, 4139 (2001).
[38]R. H. French, J. Am. Ceram. Soc. **73**, 477 (1990).
[39]H. Momida, T. Hamada, Y. Takagi, T. Yamamoto, T. Uda, and T. Ohno, Phys. Rev. B. **73**, 054108 (2006).
[40]H. Y. Yu, M. F. Li, and D. L. Kwong. Thin Solid Films. **462**, 110 (2004).
[41]H. Y. Yu, M. F. Li, B. J. Cho, C. C. Yeo, M. S. Joo, D.-L. Kwong, J. S. Pan, C. H. Ang, J. Z. Zheng, and S. Ramanathan, Appl. Phys. Lett. **81**, 376 (2002).
[42]N. V. Nguyen, O. A. Kirillov, W. Jiang, W. Wang, J. S. Suehle, P. D. Ye, Y. Xuan, N. Goel, K.-W. Choi, W. Tsai, and S. Sayan. Appl. Phys. Lett. **93**, 082105 (2008).
[43]O. Blank, H. Reisinger, R. Stengl, M. Gutsche, F. Wiest, V. Capodieci, J. Schulze, and I. Eisele, J. Appl. Phys. **97**, 044107 (2005).
[44]M. Yoshitake, W. Song, J. Libra, K. Masek, F. Sutara, V. Matolin, and K. C. Prince, J. Appl. Phys. **103**, 033707 (2008).
[45]S. Suzer, S. Sayan, M. M. Banaszak Holl, E. Garfunkel, Z. Hussain, and N. M. Hamdan. J. Vac. Sci. Technol. A **21**, 106 (2003).
[46]F. Bernardini, V. Fiorentini, and D. Vanderbilt, Phys. Rev. B **56**, 10024 (1997).
[47]F. Bernardini and V. Fiorentini, Phys. Status Solidi B **216**, 391 (1999).
[48]A. Zoroddu, F. Bernardini, P. Ruggerone, and V. Fiorentini, Phys. Rev. B **64**, 045208 (2001).
[49]U. Karrer, O. Ambacher, and M. Stutzmann, Appl. Phys. Lett. **77**, 2012 (2000).
[50]V.M. Bermudez, J. Appl. Phys. **80**, 1190 (1996).
[51]M. Krawczyk, L. Zommer, A. Jablonski, I. Grzegory, and M. Bockowski, Surf. Sci. **566–568**, 1234 (2004).
[52]O. Bierwagen, J. S. Speck, T. Nagata, T. Chikyow, Y. Yamashita, H. Yoshikawa, and K. Kobayashi, Appl. Phys. Lett. **98**, 172101 (2011).
[53]T. E. Cook, C. C. Fulton, W. J. Mecouch, R. F. Davis, G. Lucovsky, and R. J. Nemanich, J. High Speed Electron. Sys. **14**, 107 (2004).
[54]R. L. Anderson, Solid-State Electron. **5**, 341 (1962).
[55]C. Tejedor and F. Flores, J. Phys. C: Solid State Phys. **11**, L19 (1978).
[56]J. Tersoff, Phys. Rev. B **30**, 4874 (1984).
[57]J. Roberston, J. Vac. Sci. Technol. B **18**, 1785 (2000).
[58]W. Mönch, Phy. Rev. Lett. **58**, 1260 (1987).
[59]W. Mönch, J. Vac. Sci. Technol. B **6**, 1270 (1988).
[60]W. Mönch, J. Appl. Phys. **109**, 113724 (2011).
[61]L. R. C. Fonseca, D. Liu, and J. Robertson, Appl. Phys. Lett. **93**, 122905 (2008).
[62]J. Bardeen, Phys. Rev. **71**, 717 (1947).
[63]M. Schlüter, Phys. Rev. B **17**, 5044 (1978).
[64]S. Hashimoto, K. Egashira, T. Tanaka, R. Etoh, Y. Hata, and R. T. Tung, J. Appl. Phys. **97**, 024911 (2005).
[65]Y. Li, W. Long, and R. T. Tang, Solid-State Commun. **151**, 1641 (2011).